back pressures that would better reproduce the thruster plume structures expected in flight conditions.

Acknowledgments

This work was supported by NASA Lewis Research Center with F. M. Curran as technical monitor. We are grateful to NASA for supplying the arcjet and power processing unit.

References

[1]Miller, D. R., "Free Jet Sources," *Atomic and Molecular Beam Methods Volume 1*, edited by G. Scoles, Oxford Univ. Press, New York, 1988, pp. 41–44.

[2]Mitra, N. K., and Fiebig, M., "Flow in a Laval Nozzle with Gas Mixtures of Disparate Molecular Masses," in *Rarefied Gas Dynamics Volume II*, edited by H. Oguchi, Univ. of Tokyo Press, 1984, pp. 655–664.

[3]Welle, R. P., Pollard, J. E., Janson, S. W., and Cohen, R. B., "One Kilowatt Hydrogen and Helium Arcjet Performance," AIAA Paper 91-2229, June 1991.

[4]Liebeskind, J. G., Hanson, R. K., and Cappelli, M. A., "Laser-Induced Fluorescence Diagnostic for Temperature and Velocity Measurements in a Hydrogen Arcjet Plume," *Applied Optics*, Vol. 32, No. 30, 1993, pp. 6117–6127.

[5]Liebeskind, J. G., Hanson, R. K., and Cappelli, M. A., "Plume Characteristics of an Arcjet Thruster," AIAA Paper 93-2530, June 1993.

[6]Chapman, S., and Cowling, T. G., *The Mathematical Theory of Non-Uniform Gases*, Cambridge Univ. Press, New York, 1970, Chap. 8, pp. 134–150.

[7]Mitra, N. K., Fiebig, M., and Schwan, W., "Quasi-One-Dimensional Nozzle Flows of Disparate Mixtures," *Physics of Fluids*, Vol. 27, No. 10, 1984, pp. 2424–2428.

[8]Curran, F. M., and Haag, T. W., "An Extended Life and Performance Test of a Low Power Arcjet," AIAA Paper 88-3106, July 1988.

[9]Curran, F. M., Bullock, S. R., Haag, T. W., Sarmiento, C. J., and Sankovic, J. M., "Medium Power Hydrogen Arcjet Operation," AIAA Paper 91-2227, June 1991.

[10]Manzella, D. H., Curran, F. M., Myers, R. M., and Zube, D. M., "Preliminary Plume Characteristics of an Arcjet Thruster," AIAA Paper 90-2645, July 1990.

[11]Crofton, M. W., Welle, R. P., Janson, S. W., and Cohen, R. B., "Temperature, Velocity and Density Studies in the 1 kW Ammonia Arcjet Plume by LIF," AIAA Paper 92-3241, July 1992.

[12]Cappelli, M. A., Liebeskind, J. G., Hanson, R. K., Butler, G. W., and King, D. Q., "A Direct Comparison of Hydrogen Arcjet Thruster Properties to Model Predictions," 23rd International Electric Propulsion Conf., IEPC-93-220, Sept. 1994.

Direct Coupling of Euler Flow Equations with Plate Finite Element Structures

Guru P. Guruswamy* and Chansup Byun†
NASA Ames Research Center,
Moffett Field, California 94035

Introduction

In recent years, significant advances have been made for single disciplines in both computational fluid dynamics (CFD) using finite difference approaches[1] and computational structural dynamics (CSD) using finite element methods (see Chap. I of Ref. 2). For aerospace vehicles, structures are dominated by internal discontinuous members such as spars, ribs, panels, and bulkheads. The finite element (FE) method, which is fundamentally based on discretization, has proven to be computationally efficient to solve aerospace structures problems. The external aerodynamics of aerospace vehicles is dominated by field discontinuities such as shock waves and flow separations. Finite difference (FD) computational methods have proven to be efficient to solve such problems.

Problems in aeroelasticity associated with nonlinear systems have been solved using both uncoupled and coupled methods.[3] Uncoupled methods are less expensive but are limited to very small perturbations with moderate nonlinearity. However, aeroelastic problems of aerospace vehicles are often dominated by large structural deformations and high-flow nonlinearities. Fully coupled procedures are required to solve such aeroelastic problems accurately.

In computing aeroelasticity with coupled procedures, one needs to deal with fluid equations in an Eulerian reference system and structural equations in a Lagrangian system. Also, the structural system is physically much stiffer than the fluid system. As a result, the numerical matrices associated with structures are orders of magnitude stiffer than those associated with fluids. Therefore, it is numerically inefficient or even impossible to solve both systems using a single system of equations. To solve this problem, Guruswamy and Yang[3] presented a numerically accurate and efficient approach for two-dimensional airfoils by independently modeling fluids using FD-based transonic small perturbation (TSP) equations and structures using modal equations and coupling the solutions only at boundary interfaces between fluids and structures. This approach has been extended for more complete flow equations on the Euler/Navier-Stokes equations.[4] The modal approach significantly reduces the number of structural unknowns to a great extent when compared to a direct use of FE equations. However, a detailed FE model is required to generate modal data particularly in the absence of experimentally measured data. One can take direct advantage of available FE data and directly couple them with flow equations. By directly using FE data, the possible errors caused by modal approximations can be avoided, and detailed results such as stresses can be computed directly.

In this work, a procedure to compute aeroelasticity by directly coupling the Euler equations for fluids and with plate finite element equations for structures is presented. The coupled equations are solved using a time-integration method. The time accuracy is maintained using moving grids that conform to aeroelastically deformed shape computed every time step. The aerodynamic forces are transferred to structures by using simple lumped load (LL) approach and also a more accurate virtual surface (VS) approach. The VS approach developed in this work can preserve the work done by aerodynamic forces due to structural deformations. The VS approach is validated by computing the aeroelastic response of a wing and comparing with experiment. All aeroelastic responses are computed at transonic Mach numbers where strong coupling between fluids and structures is required.

Fluid-Structural Interfaces

The finite element matrix form of the aeroelastic equations of motion can be written as

$$[M]\{\ddot{q}\} + [G]\{\dot{q}\} + [K]\{q\} = \{Z\} \tag{1}$$

where $[M]$, $[G]$, and $[K]$ are the global mass, damping, and stiffness matrices, respectively. $\{Z\}$ is the aerodynamic force vector corresponding to the nodal displacement vector $\{q\}$. The aerodynamic force vector $\{Z\}$ is computed by solving Euler flow equations using ENSAERO. The plate option of the ANS4 shell/plate element is used to represent the structural properties of the wing configuration.[5]

The main effort after selecting the FE model of the structure falls into computing the global force vector $\{Z\}$ of Eq. (1). $\{Z\}$ is computed by solving the Euler equations at given time t. First, the pressures are computed at all surface grid points. The forces corresponding to the nodal DOF are computed using the fluid-structural interfaces discussed in the following section.

In aeroelastic analysis, it is necessary to represent equivalent aerodynamic loads at the structural nodal points and to represent de-

Presented as Paper 93-3087 at the AIAA 24th Fluid Dynamics Conference, Orlando, FL, July 6–9, 1993; received July 26, 1993; revision received April 7, 1994; accepted for publication April 7, 1994.

*Research Scientist, Computational Aerosciences Branch. Associate Fellow AIAA.

†Research Scientist, MCAT Institute, Computational Aerosciences Branch. Member AIAA.

formed structural configurations at the aerodynamic grid points. In the present domain decomposition approach, coupling between the fluid and structural domains is achieved by combining the boundary data such as aerodynamic pressures and structural deflections at each time step. An analytical moving grid technique has been successfully used to deform the aerodynamic grid according to structural deflections at the end of every time step. There are several different ways to obtain the global force vector $\{\mathbf{Z}\}$ of Eq. (1) depending on the equations used for the structural dynamic analysis.

A number of numerical procedures have been developed to exchange the necessary information between the aerodynamic and structural domains as listed in Ref. 6. Use of a bilinear interpolation and a VS interface are investigated in this study. The bilinear interpolation is same as the LL approach. In this approach, the force acting on each element of the structural mesh is first calculated, and then the element nodal force vector is obtained by distributing the total force. The global force vector is obtained by assembling the nodal force vectors of each element. In addition, the deformed configuration of the CFD grid at the surface is obtained by linearly interpolating nodal displacements at finite element nodes. This approach does not conserve the work done by the aerodynamic forces and needs fine grids for both fluids and structures to give accurate results.

An alternate to the LL approach is an improved approach based on the VS. In this approach, a mapping matrix developed by Appa[6] is selected to accurately exchange data between the fluid and structural interface boundaries. The reason for selecting Appa's method is that the mapping matrix is general enough to accommodate changes in fluid and structural models easily. In addition, this approach conserves the work done by aerodynamic forces when obtaining the global nodal force vector. This method introduces a VS between the CFD surface grid and the finite element mesh for the wing. This VS is discretized by a number of finite elements, which are not necessarily the same elements used in the structural surface modeling.

By forcing the deformed VS to pass through the given data points of the deformed structure, a mapping matrix relating displacements at structural and aerodynamic grid points is derived as

$$[T] = [\psi_a]\left(\delta^{-1}[K] + [\psi_s]^T[\psi_s]\right)^{-1}[\psi_s]^T \tag{2}$$

where $[K]$ is the free-free stiffness of the VS, ψ_s is displacement mapping from VS to structural grids, ψ_a is displacement mapping from VS to aerodynamic grids, and δ is the penalty parameter.

Then, the displacement vector at the aerodynamic grid $\{q_a\}$ can be expressed in terms of the displacement vector at the structural nodal points q_s as

$$\{q_a\} = [T]\{q_s\} \tag{3}$$

From the principle of virtual work, the nodal force vector $\{\mathbf{Z}_s\}$ can be obtained as

$$\{\mathbf{Z}_s\} = [T]^T\{\mathbf{Z}_a\} \tag{4}$$

where $\{\mathbf{Z}_a\}$ is the force vector at the aerodynamic grids. This procedure is illustrated in Fig. 1.

The aeroelastic equation of motion Eq. (1) is solved by a numerical integration technique based on the constant-average-acceleration method. To maintain the time accuracy, grids are regenerated every time step according to the aeroelastically deformed shape by using the moving grid capability available in Computer Code ENSAERO.

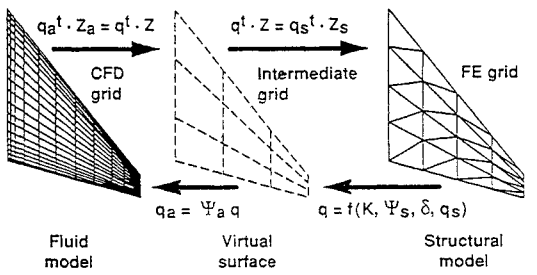

Fig. 1 Fluid-structure interfacing using virtual surface approach.

Results

To demonstrate aeroelastic computations, a typical fighter type wing is selected. For this wing transonic flutter data is available from wind-tunnel tests.[7] In this computation, the flowfield is discretized using a C-H grid topology of size 151 × 30 × 35.

This is the first time a plate FE model has been directly coupled with the Euler equations. As a result, the validity of the coupling approach will be verified by comparing the FE results with those from the previously well-validated modal analysis. In this calculation, the FE computations were made using 36 plate elements, and the modal computations were made using the first six modes of the wing. Six elements each were assigned along the chordwise and spanwise directions, respectively. Figure 2 shows the displacement responses of the leading edge at the tip obtained by both FE and modal analyses for $M_\infty = 0.854$, $p = 0.70$ psi, and $\alpha = 1.0$ deg. For this simulation, dynamic aeroelastic computations were made setting a high value for the damping coefficient so that the final results would approach steady-state conditions. The VS approach was used to calculate nodal forces for both the FE and modal analysis. Results in Fig. 2 demonstrate the validity of the coupling of plate elements with the Euler equations. The FE approach gives displacements about 0.1% higher than the modal approach. Such results are expected since the modal approach yields a structure that is stiffer than the actual one, whereas the FE approach represents the actual structural stiffness.

The accuracy of the results can depend on the type of interfaces between fluids and structures. In the following calculations, the simple LL and the more accurate VS interfaces are compared to each other, and the results are shown in Fig. 3. The wing structure was modeled using 100 ANS4 elements. An assignment of 10 elements each was made along the chordwise and spanwise directions, respectively. To discretize the VS, a four-noded, isoparametric element is used. For a given dynamic pressure of 1.0 psi and initial acceleration of 1.0×10^5 in./s, the time history of total lift on the wing is presented in Fig. 3. The total lift obtained by integrating the pressure coefficients at CFD grid points is also shown in the figure. The total lift using CFD grid points is more accurate than those from VS and

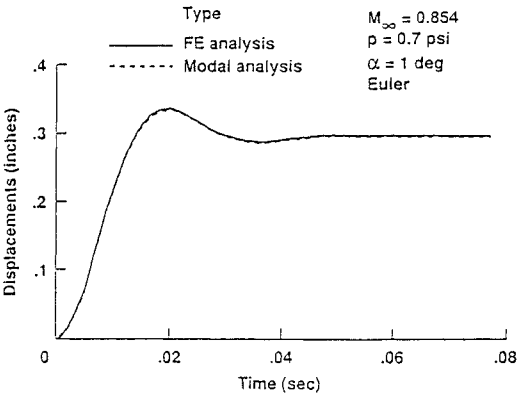

Fig. 2 Validation of finite element implementation in ENSAERO.

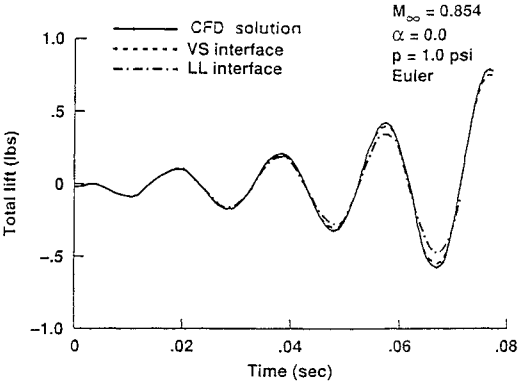

Fig. 3 Comparison of lumped load and virtual surface interfacing methods.

LL methods. Both VS and LL approaches obtain the total lift by summing the forces at the FE nodal points, which was transformed from the pressure coefficients through interfaces. The VS approach transfers pressure data more accurately than the LL approach. The LL approach shows that the response around peaks deviates from the CFD solution. For this case the LL approach shows reasonable agreement with the VS approach.

The present work has strong potential for general applications dealing with more complex geometries and complete equations. Application of this approach for wing-body configurations by using the Navier–Stokes equations is demonstrated in Ref. 8.

References

[1]Holst, T. L., Flores, J., Kaynak, U., and Chaderjian, N., "Navier-Stokes Computations, Including a Complete F-16 Aircraft," *Applied Computational Aerodynamics*, edited by P. A. Henne, Vol. 125, Progress in Astronautics and Aeronautics, AIAA, Washington, DC, 1990, Chap. 21.

[2]Yang, T. Y., *Finite Element Structural Analysis*, Prentice-Hall, Englewood Cliffs, NJ, 1986.

[3]Guruswamy, P., and Yang, T. Y., "Aeroelastic Time Response Analysis of Thin Airfoils by Transonic Code LTRAN2," *Computers and Fluids*, Vol. 9, No. 4, 1980, pp. 409–425.

[4]Guruswamy, G. P., "ENSAERO–A Multidisciplinary Program for Fluid/Structural Interaction Studies of Aerospace Vehicles," *Computing System Engineering*, Vol. 1, Nos. 2–4, 1990, pp. 237–256.

[5]Park, K. C., Pramono, E., Stanley, G. M., and Cabiness, H. A., "The ANS Shell Elements: Earlier Developments and Recent Improvements," *Analytical and Computational Models of Shells*, edited by A. K. Noor, T. Belytschko, and J. C. Simo, CED-Vol. 3, American Society of Mechanical Engineers, New York, 1989, pp. 217–240.

[6]Appa, K., "Finite-Surface Spline," *Journal of Aircraft*, Vol. 26, No. 5, 1989, pp. 495, 496.

[7]Dogget, R. V., Rainey, A. G., and Morgan, H. G., "An Experimental Investigation of Aerodynamics Effects of Airfoil Thickness on Transonic Flutter Characteristics," NASA TM X-79, Nov. 1959.

[8]Guruswamy, G. P., and Byun, C., "Fluid-Structural Interactions Using Navier-Stokes Flow Equations Coupled With Shell Finite-Element Structures," AIAA Paper 93-3087, July 1993.

Shear Buckling of Simply Supported Skew Mindlin Plates

Y. Xiang*
University of Queensland, Brisbane 4072, Australia
C. M. Wang†
National University of Singapore, Kent Ridge, 0511 Singapore
and
S. Kitipornchai‡
University of Queensland, Brisbane 4072, Australia

Introduction

THERE are two kinds of in-plane shear loadings in shear buckling analysis of skew plates. The first kind of shear loading is that along the two horizontal edges where the traction is a pure shear stress, whereas along the other two oblique edges, the traction consists of both shear and direct stresses of such magnitude that every infinitesimal rectangular element is in a state of pure shear. Another kind of shear buckling considered for skew plates is where the shear loads are uniformly applied along the plate edges. Figure 1 shows these two kinds of shear loadings, and we refer to the first kind of shear loading as R shear loading and the second kind as S shear loading in this Note. The geometry of the plate is also given in Fig. 1a.

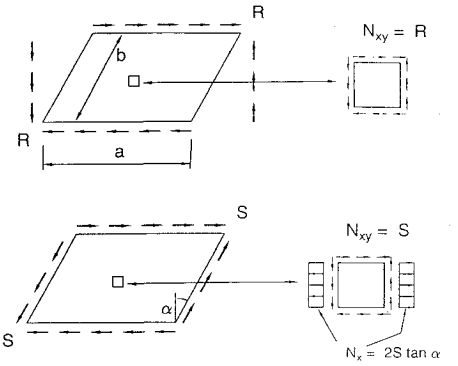

Fig. 1 Two kinds of shear loading conditions on skew plates: a) *R* shear loading and b) *S* shear loading.

Since 1954, the shear buckling of skew plates has been studied by a number of researchers such as Wittrick,[1] Argyris,[2] Durvasula,[3] and Yoshimura and Iwata.[4] These studies, however, were all confined to thin skew plates based on the Kirchhoff plate theory. When the plates are thick, these thin plate solutions overpredict the shear buckling load, and the error increases with increasing plate thickness. The error is, due to the neglect of shear deformation in thin plate theory.

Based on the Reissner–Mindlin[5,6] shear deformation plate theory and applying the pb-2 Rayleigh–Ritz solution procedure,[7,8] this Note presents critical shear load factors (for R and S shear loadings) for simply supported skew Mindlin plates of various aspect ratios a/b, skew angles α, and thickness-length ratios h/b. Note that the potential energy functional of skew Mindlin plates was derived in skew coordinates. The derivation of the formulation and the solution process have been detailed in Ref. 8. The shear correction factor $\kappa = 5/6$ and Poisson's ratio $\nu = 0.3$ are used where required.

Results and Discussion

The in-plane forces on an infinitesimal rectangular element are given by (see Fig. 1) for R shear loading

$$N_{xy} = R \text{ and } N_x = 0 \tag{1a}$$

and for S shear loading

$$N_{xy} = S \text{ and } N_x = 2S\tan\alpha \tag{1b}$$

and the shear buckling factors are for R shear loading

$$\lambda = \lambda_R = \frac{Rb^2}{\pi^2 D} \tag{2a}$$

and for S shear loading

$$\lambda = \lambda_S = \frac{Sb^2}{\pi^2 D} \tag{2b}$$

where $D = Eh^3/[12(1-\nu^2)]$ is the flexural rigidity of the plate.

Skew plates of various aspect ratios a/b, skew angles α, and thickness to oblique width ratios h/b have been considered.

Based on convergence studies, it has been found that 14th degree polynomials in the pb-2 trial functions are sufficient to ensure converged solutions. Since no shear buckling solutions for thick plates are available, comparisons can only be made with thin plate solutions. Plates with $h/b = 0.001$ may be regarded as thin plates since the shear deformation effect is almost negligible. Table 1 shows the shear buckling solutions of such thin plates with results obtained by previous researchers. Generally, the present results are in close agreement with existing solutions except for some cases (for example, $\alpha = -30$ deg). The authors believe that some of the previously published solutions may not have quite converged. The comparison studies verify somewhat the validity of the present formulation and analysis and the accuracy of the results.

Received May 22, 1993; revision received March 11, 1994; accepted for publication March 17, 1994.

*Postdoctoral Research Fellow, Department of Civil Engineering.
†Senior Lecturer, Department of Civil Engineering.
‡Professor, Department of Civil Engineering.